15 (2022) 100109

Contents lists available at ScienceDirect

Journal of Non-Crystalline Solids: X

journal homepage: www.sciencedirect.com/journal/journal-of-non-crystalline-solids-x

Alkali and alkaline earth zinc and lead borate glasses: Structure and properties

Lina Heuser *, Marianne Nofz

Bundesanstalt für Materialforschung und -prüfung (BAM), Berlin, Germany

ARTICLE INFO

Keywords:
Raman spectroscopy
IR spectroscopy
Alkali zinc borate glasses
Lead borate glasses
Physical properties
Young's Modulus

ABSTRACT

Low melting Li_2O-PbO-B_2O_3, Me_2O-ZnO-B_2O_3, Me = Li, Na, K, Rb and CaO-ZnO-B_2O_3 glasses were studied with Raman and infrared spectroscopies to advance the structural understanding of zinc borate glasses as potential candidates for substitution of lead containing glasses.

Although the effect of type of alkali ions on the number (N_4) of fourfold coordinated boron (B_4) in the glasses is small, the alkali ions direct the type of borate groups, i.e., pentaborate in lithium, sodium, and calcium zinc borate glasses, as well as diborate in potassium and rubidium containing ones. Both groups were simultaneously found in Li_2O-PbO-B_2O_3. Alkali ions are mainly responsible for the formation of B_4-units and metaborate. Zinc ions favorably compensate non-bridging oxygen and partially form ZnO_4.

With decreasing N_4 and field strength of the alkali ions the atomic packing density, glass transition temperature and Young's Modulus also decrease. The coefficient of thermal expansion increases with decreasing N_4.

1. Introduction

Due to the non-toxic behavior and high polarizability [1,2] ZnO is a suitable candidate to substitute PbO in glasses for the application in optical materials and optoelectronics [1,3–7]. The same argument led to the development of lead-free Ag-metallization pastes, e.g. for application in photovoltaics [8–10], low temperature cofired ceramics (LTCC) [11,12], or in sealants and solders [2,13]. Additionally, the compactness of the structural network and the mechanical properties are enhanced in Zn containing alkali borate glasses [14].

Based on these ideas, in the present study low melting alkali and alkaline earth containing zinc borate glasses are investigated with the aim to replace lead containing paste glasses in photovoltaics. A lead containing lithium borate glass serves as a reference here. ZnO was partially substituted by CuO to study the effect of Cu^{2+} in glass-bearing metallization paste to enhance glass stability and homogeneity of the borate network [15].

To understand the relations between composition and properties of multicomponent zinc borate glasses as a prerequisite for the development of materials with specific properties Raman as well as IR [1–3,7,15–20] and partially also NMR [18] spectroscopies were used. As known from the very detailed studies of binary borate glasses [21–36], boron may appear in threefold (B_3) and fourfold (B_4) coordination and these polyhedra may combine to different borate groups [37–39]. Additionally, non-bridging oxygen (NBO) may occur and form e.g., metaborate rings and chains or pyroborate groups or others [21,26,37]. Studies of binary alkali borate glasses allowed to find relations between composition and type of borate groups detectable in the glasses [21,37]. Thus more than ten distinguishable borate groups were discussed e.g. by Konijnendijk and Stevels [21], and Kamitsos and Chryssikos [26].

Addition of zinc oxide to binary alkali or alkaline earth borate glasses could induce a competition between the cations for charge compensation of borate-units. The competition of alkali or alkaline earth and zinc ions in glasses of metaborate composition is rarely described in the available literature, merely a work on lithium containing zinc metaborate glass [7] can be mentioned here.

Zn^{2+} can occur as network former in fourfold coordination or as network modifier in sixfold coordination [5,15,40]. From literature it is not clear, if ZnO is also able to compensate the negative charge of B_4-units as found in [7], to the opposite favored trigonal B_3 with NBO [3] or if ZnO has no influence on the transition of B_3 in B_4 [2]. Spectroscopic studies based on the variation of the type of alkali ion in ternary zinc borate glasses are missing.

From the binary borate glasses it is known, that the relation between formation of either B_4 or NBO significantly determines e.g. the transition temperature (T_g) and the coefficient of thermal expansion (CTE)

* Corresponding author at: Bundesanstalt für Materialforschung und -prüfung (BAM), Richard-Willstätter-Str. 11, 12489 Berlin, Germany.
E-mail addresses: Lina.Heuser@bam.de (L. Heuser), Marianne.Nofz@bam.de (M. Nofz).

https://doi.org/10.1016/j.nocx.2022.100109
Received 12 May 2022; Received in revised form 24 June 2022; Accepted 1 August 2022
Available online 6 August 2022

[24,25]. Due to the manifold of possible borate groups in ternary glasses, simple relations between composition, structure and properties are not expected. The present work aims on the identification of borate groups in ternary borate glasses by means of combination of IR and Raman spectroscopies as a prerequisite for understanding the influence of the different constituents of the networks on physical including mechanical properties. Thus, in the present study, the consequences of the variation of the network modifiers in zinc borate glasses and of the replacement of ZnO by PbO or CuO are analyzed.

Surprisingly, though the effect of the type of alkali ion on the number of B_4 containing borates (N_4) in the ternary zinc borate glasses is small, the alkali ions direct the formation of B_4 containing borate groups. Based on the structural changes, the glasses could be divided into two groups: The first one comprises samples with the alkali ions Li^+ or Na^+ and the second one K^+ or Rb^+ containing glasses. A linear decrease of the B_4-content of the glasses with lower field strength of the alkali will be presented. Relations between properties, e.g., T_g, atomic packing density (APD), as well as Young's Modulus, and B_4-content will be figured out.

2. Experimental

2.1. Samples

The influence of network modifier on structure-property-relations was studied for Me_2O-ZnO-B_2O_3, Me = Li, Na, K, Rb (MeZB) glasses and CaO-ZnO-B_2O_3 (CaZB) glass. The rubidium content was diminished concomitant with increased borate content for RZB1 glass. To focus the role of intermediate oxides on structure and properties, zinc oxide was partially replaced by copper oxide yielding Na_2O-ZnO-CuO-B_2O_3 (NZCuB) glass and completely replaced by lead oxide yielding Li_2O-PbO-B_2O_3 (LPbB) glass.

2.1.1. Glass melts

The borate glasses were prepared from the raw materials Li_2CO_3 (Emplura ≥98.5%, Merck KGaA, Darmstadt, Germany), Na_2CO_3 (Ensure ISO ≥99.9%, Merck KGaA, Darmstadt, Germany), K_2CO_3 (p.a. ≥99.9%, Merck KGaA, Darmstadt, Germany), Rb_2CO_3 (99%, ChemPUR GmbH, Karlsruhe, Germany), $CaCO_3$ (p.a. ≥99.5%, Merck KGaA, Darmstadt, Germany), ZnO (≥99%, Carl Roth GmbH, Karlsruhe, Germany), PbO (p.a. ≥99%, yellow, Honeywell, Fluka, Seelze, Germany), CuO (p.a. ≥99%, Honeywell, Fluka, Seelze, Germany) and B_2O_3 (99%, Alfa Aesar/ ThermoFisher (Kandel) GmbH, Kandel, Germany).

The compositions are given in the results part. 1.700 kg to 3.500 kg batches of LZB, NZB, KZB, and RZB1 were melted in an inductively heated furnace (Ema Tec 2002, EMA Tec GmbH, Sondershausen, Germany) at 1100 °C for 1 h in Pt/Rh 20 crucibles. In a high temperature laboratory furnace VMK1800 (Linn High Therm GmbH, Eschenfelden, Germany) 0.050 kg to 0.450 kg batches of RZB were prepared at 1100 °C for 1 h in Pt/Rh 20 crucibles, CaZB at 1250 °C for 1 h in Pt/Rh 20 crucibles, LPbB at 950 °C for 1 h in Al_2O_3 crucibles, NZCuB at 1100 °C for 1 h in Al_2O_3 crucibles. Because of their strong crystallization tendency, homogenization and powder preparation, the melts were fritted in water, despite CaZB.

2.1.2. Bulk glass samples

CaZB was directly obtained as ingot from the melt. The other bulk glass samples were made from glass frits remelted and casted onto steel, except LZB, which was casted onto copper molds. Casted glass plates were heated to at least 20 K above T_g of each glass and cooled to room temperature in the switched off furnace without dwell time.

2.1.3. Glass powders

Glass frits were dry milled in air for 12 min with a planetary micro mill (Pulverisette 7, Fritsch, Idar-Oberstein, Germany) equipped with zirconium oxide (ZrO_2) grinding jars filled with ZrO_2 balls, D = 10 mm. To prevent particle agglomeration, 0.01 wt% methanol was added.

2.2. Methods

2.2.1. Glass composition

The chemical composition of glasses was analyzed by means of Inductively Coupled Plasma-Optical Emission Spectrometry (ICP-OES 5100, Agilent Technologies, Waldbronn, Germany) based on DIN 51086–2 [41]. Dry milled glass powders sieved to <63 μm were dispersed in an acid mixture of HNO_3, H_3PO_4 and HF and dissolved in an autoclave (TurboWave, MLS GmbH, Leutkirch, Germany) for this study.

2.2.2. Glass density

To determine the density ρ of the glasses, the Archimedes' principle was used with water as immersion liquid at room temperature. Bulk glass samples, ((5 or 4) × (5 or 4) × 25) mm^3 in size, cut from the casted glass plates, were utilized. The average of 10 measurements of each sample was calculated. The low weight of the samples caused an uncertainty in the third digit.

2.2.3. Glass transition temperature and coefficient of thermal expansion

For horizontal dilatometry the in paragraph 2.2.2 mentioned samples were used. The glass transition temperature, T_g, and the coefficient of thermal expansion, CTE, were measured with a horizontal dilatometer equipped with a quartz glass measuring head (DIL 402c, Netzsch-Gerätebau GmbH, Selb, Germany) for two glass samples of each composition. These samples were first heated at 5 K/min about T_g, cooled to room temperature with 5 K/min and again heated for T_g measurement. The mean value was calculated using the second measurement of each the two samples of each composition. Additionally, T_g was measured with differential thermal analysis (DTA) (TAG 24, Setaram, Caluire, France). 10 mg–20 mg glass powder were heated to nearly T_g + 50 K in air using Pt-crucibles, except Al_2O_3 crucibles for LPbB. The heating rate of 10 K/min was selected for DTA corresponding to 5 K/min for dilatometry [42]. Three heating and cooling cycles were performed for each sample.

2.2.4. Young's Modulus

The elastic properties of glass samples with size of approx. (50 × 5 × 3) mm^3 or (50 × 15 × 3) mm^3 were measured at room temperature on the basis of ASTM E-1876-15 [43] using a resonance frequency damping analyzer (RFDA basic Version 1.4, IMCE nv, Genk, Belgium). The sample was stimulated by a small mechanical impulse to measure in flexural and for the larger samples to measure in torsional mode. The measurement was repeated 10 times for each sample and the mean values are determined. For the flexural mode, the Poisson's ratio ν was set to 0.275. A microphone (RFDA basic microphone, IMCE nν, Genk, Belgium) recorded the resonance frequency. The Young's Moduli E, and for the larger samples the shear moduli G and Poisson's ratios ν were calculated with the software RFDA-MF basic v.1.2.0., according to ASTM E-1876-15 [43].

2.2.5. Glass structure

The glass structure was analyzed by means of the complementary methods Raman spectroscopy and infrared spectroscopy.

2.2.6. Raman spectroscopy

Raman spectra of polished bulk glass samples were studied with a LabRam HR 800 instrument (Horiba132 Jobin Yvon, Bensheim, Germany) combined with a microscope (BX41, Olympus, Tokyo, Japan). At three different sites spectra were recorded for each glass. At each site two spectra were recorded with a measuring time of 30 s for the alkali zinc borate glasses, four spectra with a measuring time of 15 s for LPbB and six spectra with a measuring time of 10 s for CaZB because of higher intensities. The wavenumber calibration was performed using a quartz standard. The spectra were measured from approx. 60 cm^{-1} to 2360

cm^{-1} with a resolution of 2 cm^{-1}. A grating of 300 grooves per mm and an objective lens with 50×/N.A. = 0.55 long working distance were used. A laser with 633 nm wavelength and approx. 9 mW power was utilized. For comparison, smoothing with 5 points, a baseline correction with a Bspline baseline as also practiced by other authors (e.g. [44]) and the normalization of the spectra were performed using the software Origin 2020 [45].

2.2.7. Infrared spectroscopy

Infrared (IR) spectra of glass powders sieved to <300 μm were measured using an Equinox 55 FT-IR spectrometer (Bruker, Ettlingen, Germany). The spectrometer was coupled with a microscope, which possessed an ATR-objective used for the measurements. The spectra of each powder sample with a resolution of 2 cm^{-1} were received in the range between 4000 cm^{-1} and 600 cm^{-1}. The IR-ATR spectra were transformed using extended ATR correction of the software OPUS (Bruker, Billerica, USA) with number of ATR reflections one, the ATR angle of incidence 45°, mean refraction index of sample of standard 1.5 and the material of ATR crystal Germanium. To achieve better comparability, smoothing with 5 points, a baseline correction with a horizontal or user defined line and the normalization of the spectra to highest intensity were applied utilizing the software Origin 2020 [45].

3. Results

3.1. Physical glass properties

Table 1 summarizes the analyzed chemical compositions of the borate glasses under study. The estimated by ICP-OES alumina content of the samples molten in corundum crucibles is below 1 mol% and will not be accounted for in the data given in Table 1.

Table 2 lists the selected physical properties of the borate glasses under study. Density, glass transition temperature, CTE and Young's Modulus were additionally calculated by SciGlass [46] using the method Priven 2000. The atomic packing density was calculated according to eq. (1) [47].

$$\mathrm{APD} = \rho \bullet \frac{\sum X_i \frac{4}{3} \pi N_A \left(c_i r_{Ai}^3 + d_i r_{Bi}^3\right)}{\sum X_i M_i} = \frac{\sum X_i \frac{4}{3} \pi N_A \left(c_i r_{Ai}^3 + d_i r_{Bi}^3\right)}{V_m} \quad (1)$$

where N_A denotes Avogadro's number, X_i the molar fraction of oxide i with the formula A_cB_d, M_i its molar mass, r_A and r_B the respective ionic radii and V_m the molar volume. The effective alkali and alkaline earth ionic radii r were taken in 6-fold coordination from Shannon [48], as given in Table 2. Radii for zinc (60 pm, 4-fold), lead (98 pm, 4-fold), cooper (57 pm, 4-fold), boron (1 pm, 3-fold) and oxygen (135 pm, 2-fold) are also given in [48].

The free molar volume $V_{m,\ free}$ was calculated with eq. (2)

$$V_{m,free} = \frac{\sum X_i M_i}{\rho} - \sum X_i \frac{4}{3} \pi N_A \left(c_i r_{Ai}^3 + d_i r_{Bi}^3\right) = V_m \left(1 - APD\right) \quad (2)$$

utilizing the APD [49].

In Table 2 Dietzel's Field strength F will be taken form ref. [50] with coordination number 6 for Li^+, Na^+, Ca^{2+}, Cu^{2+}, Pb^{2+} and 8 for K^+, Rb^+.

The density of the alkali zinc borate glasses decreases with increasing alkali ionic radius, except for RZB. Ca^{2+} instead of alkali ions results in a higher density, as well as the substitution of Zn^{2+} by Pb^{2+}. The free volume $V_{m,\ free}$, and the molar volume behave in an opposing trend to the APD, so that $V_{m,\ free}$ and V_m increase with increasing ionic radius $Li^+ < Na^+ < K^+ < Rb^+$. V_m and $V_{m,\ free}$ of CaZB are similar to LZB. Comparing LZB and LPbB, the intermediate oxide Pb^{2+} with a larger radius than Zn^{2+} causes a higher $V_{m,\ free}$. Zn^{2+} substituted by 5 mol% Cu^{2+} in NZCuB results in smaller change of $V_{m,\ free}$ due to similar ionic radii of Cu^{2+} and Zn^{2+} and similar glass densities. T_g decreases with increasing alkali ionic radius and T_g increases for CaZB. T_g decreases for LPbB in comparison to LZB. CTE increases with increasing alkali ionic radius and decreases for CaZB. CTE of LPbB is higher than that of LZB. E decreases with increasing alkali ionic radius significantly stronger than expected from SciGlass calculation [46]. Using Pb^{2+} instead of Zn^{2+} as intermediate oxide, the Young's Modulus decreases and increases for Ca^{2+} instead of the alkali ions.

3.2. Raman spectroscopy

The raw data of Raman spectra of the LPbB and CaZB glasses result due to a strong fluorescence in diagonal courses shown in Fig. S1 a.) in the supplemental material. Fluorescence is less in the alkali containing glasses shown in Fig. S1 b.). For better comparability, the smoothed, baseline corrected, and normalized Raman spectra are shown together in Fig. 1. In contrast to the alkali zinc borate glasses with their highest intensities at ~775 cm^{-1}, LPbB and CaZB have their highest intensities at 1373 cm^{-1} and 1273 cm^{-1}, respectively.

For the description of the spectral features three wavenumber regions shall be considered.

i. The first comprises broad, weak, and superimposed bands in the region between 200 cm^{-1} and 580 cm^{-1}. It is conspicuous, that the spectra of LZB, NZB (Fig. 1) and CaZB (Fig. 2) are very similar in that region with the maximum at ~453 cm^{-1} and different from KZB and RZB as seen at 498 cm^{-1} and 540 cm^{-1}. Only weak bands were detected in that region for LPbB.
ii. Between about 580 cm^{-1} and ~ 1100 cm^{-1} the bands of CaZB and LPbB appear to be small in the normalized spectra depicted in Fig. 1. This is due to the normalization with respect to the strongest bands which are those above 1100 cm^{-1} in case of the CaZB and LPbB. Fig. 2 enables a better comparison of the spectra of CaZB, LPbB, and LZB. Therefore, a section from 200 cm^{-1} to 1080 cm^{-1} was enlarged for LPbB- and CaZB-spectra in comparison to the LZB-spectrum. The spectra are normalized to the highest band in the section, respectively. The strongest band of LZB at 775 cm^{-1} in this section appears also in CaZB and in LPbB, but in LPbB the strongest band is at 729 cm^{-1}. In the LPbB spectrum the bands between 600 cm^{-1} and 730 cm^{-1} are shifted and are partially stronger than for LZB, while the bands between 850 cm^{-1} and 1040 cm^{-1} have all a similar intensity in the LPbB spectrum.
iii. For alkali containing glasses the strongest bands are systematically shifted with increasing ionic radius and weight of the alkali

Table 1
Chemical composition in mol%, measured by means of ICP-OES.

Glass	Li_2O	Na_2O	K_2O	Rb_2O	PbO	CaO	CuO	ZnO	B_2O_3
LZB	19.9							26.9	53.2
NZB		19.9						26.4	53.7
KZB			19.1					27.6	53.3
RZB				19.4				27.1	53.5
RZB1				14.9				26.2	58.9
LPbB	19.5				25.2				55.3
CaZB						18.4		31.1	49.5
NZCuB		20.8					4.7	21.9	52.6

Table 2
Measured physical properties of the zinc and lead borate glasses, calculated by SciGlass [46] properties (calc.) and respective percental differences Δ.

Property	Unit	LZB	NZB	KZB	RZB	RZB1	LPbB	CaZB	NZCuB
ρ	(± 0.008) [g/cm^3]	2.829	2.788	2.632	3.020	2.996	3.764	3.103	2.764
ρ_{calc}	[g/cm^3]	2.802	2.819	2.788	3.167	3.042	4.033	3.121	2.801
Δρ	[%]	−0.96	1.10	5.91	4.88	1.53	7.15	0.57	1.32
V_m	[cm^3/mol]	22.93	25.54	29.47	31.65	30.10	26.72	22.94	25.82
$V_{m,free}$		9.54	11.47	13.97	15.22	13.79	12.61	9.89	11.88
APD	–	0.584	0.551	0.526	0.519	0.542	0.528	0.569	0.540
T_g, Dil.	(± 5) [°C]	467	465	452	444	444	399	580	458
T_g, DTA		472	465	460	448	449	394	583	463
$T_{g,\ calc}$	[°C]	493	466	432	414	429	447	598	465
ΔT_g	[%]	5.79	0.43	−4.21	−6.76	−3.38	11.5	3.1	1.53
CTE*	(± 0.25) [10^{-6} K^{-1}]	8.54	9.91	11.5	12.0	11.5	9.46	7.09	9.63
CTE_{calc}	[10^{-6} K^{-1}]	7.98	10.4	11.6	11.9	10.3	9.69	6.85	11.0
ΔCTE	[%]	−6.56	4.94	0.87	−0.83	−10.4	2.43	−3.39	14.2
E	(± 0.1) [GPa]	92.5	66.5	46.3	38.1	42.2	74.6	95.2	65.3
E_{calc}	[GPa]	87.2	71.2	63.4	62.1	64.8	74.2	100	68.5
ΔE	[%]	−5.73	7.07	36.93	62.99	53.55	−0.54	5.04	4.9
G	(± 0.1) [GPa]	–	–	–	15.0	16.7	–	–	25.5
ν	(± 0.001)	–	–	–	0.285	0.314	–	–	0.274
r‡ [48]	[pm]	76	102	138	152	152	98	100	57
F [50]	[Å^{-2}]	0.23	0.19	0.13	0.12	0.12	0.34	0.35	0.53

*CTE up to 400 °C, except LPbB up to 300 °C and CaZB up to 500 °C due to different T_g
‡Effective ionic radius r of the alkali ions and alkaline earth ion Ca^{2+} for coordination number 6, Cu^{2+} and Pb^{2+} 4-fold coordinated.

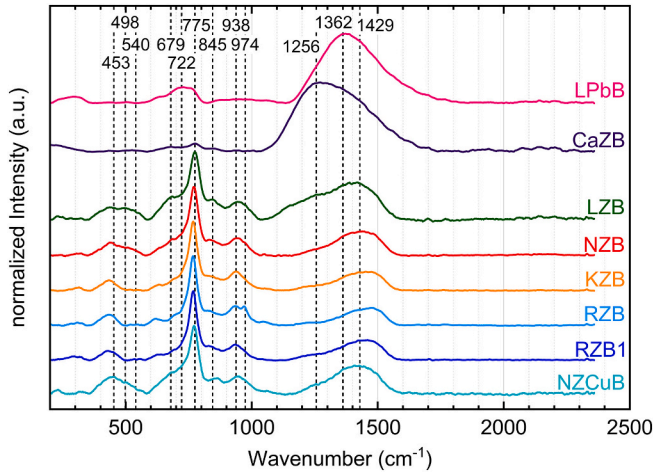

Fig. 1. Baseline corrected and normalized Raman spectra of the borate glasses under study, characteristic wavenumbers are marked with dashed lines.

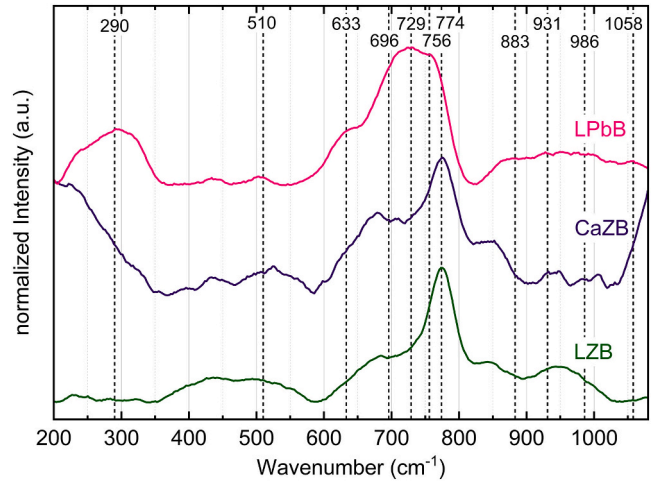

Fig. 2. Raman spectra of LZB, LPbB and CaZB, each normalized to the highest intensity in the shown section, bands of LPbB are marked with dashed lines.

ions from 775 cm^{-1} for Li^+ to 767 cm^{-1} for Rb^+. As shown before normalization in Fig. S1b), the strongest bands become sharper and higher with increasing alkali ionic radius. Although the spectra of the alkali zinc borate glasses are similar to each other, they can again be separated into two groups due to the intensities between 600 cm^{-1} and 740 cm^{-1}. These are higher for LZB + NZB than for KZB + RZB. The bands at ~938 cm^{-1} and ~ 974 cm^{-1} are only separated in RZB. The bands at 679 cm^{-1} and 845 cm^{-1} decrease with increasing alkali ion radius and appear also in CaZB.

iv. All spectra show broad, superimposed bands in the region 1100 cm^{-1}-1700 cm^{-1} which are strongest for CaZB and LPbB.

Spectra of LZB and RZB were, due to their representative character for the two groups of alkali zinc borate glasses distinguished above, selected for further consideration.

Fig. 3 shows the results of fitting of the Raman spectra of LZB and RZB glass with Lorentz alignment in accordance with [51] using the software Origin 2020 [45].

To do so, the normalized spectra were split into three parts: (i) ~200 cm^{-1}- ~ 580 (570, RZB) cm^{-1}, (ii) ~580 (570, RZB) cm^{-1}- ~ 1040 cm^{-1} (1112 cm^{-1} RZB), and (iii) ~1040 cm^{-1} (1112 cm^{-1} RZB)- ~ 1650 (1600, RZB) cm^{-1}.

Fig. 3 and Table S 1 in the supplemental material present the peak centers of the bands in the Raman spectra of LZB and RZB. The peak centers of bands 2, 8 15, 18 and 22 are similar for LZB and RZB within the wavenumber uncertainty. The bands 11, 14, 17, 21 and 23–24 are shifted to higher wavenumbers for LZB, and the band 4–7 and 12–13 are shifted to higher wavenumbers for RZB. The first bands 0–1, the bands 9–10, 16 and 20 are missing in the RZB spectrum, while the bands 3, 19 and 25 are missing in the LZB spectrum.

3.3. *Infrared spectroscopy*

Fig. S2 (supplemental material) shows the raw data of ATR-IR spectra of the glasses under study. In contrast to the Raman spectra no significant differences between the IR spectra of alkali and Ca or Pb containing glasses appear.

Fig. 4 shows the smoothed and normalized infrared spectra of the glasses obtained after transformation of ATR data.

The dashed lines indicate bands of the LZB spectrum according to the deconvolution shown below. The highest, broad region is located

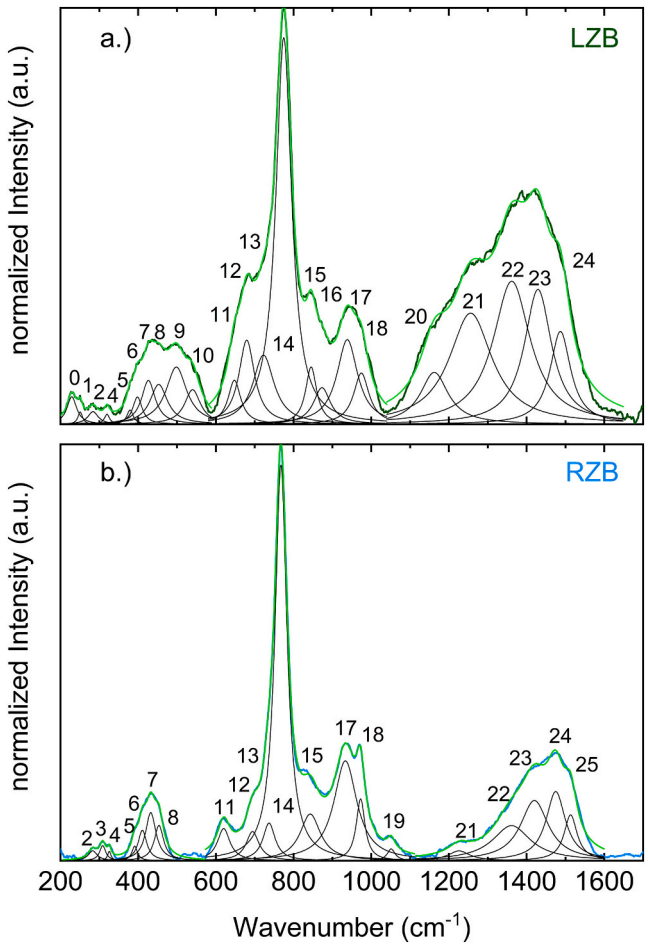

Fig. 3. Fit with Lorentz alignment of the Raman spectra of a.) LZB and b.) RZB, bands are numbered adapted to the peak centers. R^2 (correlation factors) were 0.991–0.998 for LZB fit and 0.983–0.999 for RZB fit.

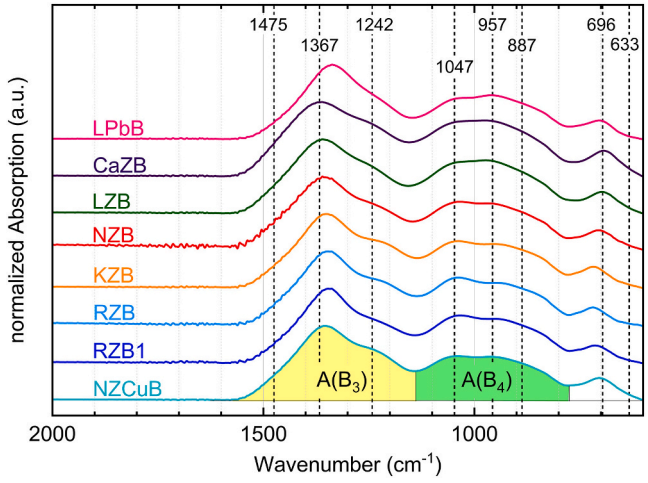

Fig. 4. IR spectra obtained after transformation of ATR data, baseline correction and normalization to the maximum absorption - at 1367 cm^{-1} for LZB - of the borate glasses under study. Bands of LZB are marked with dashed lines. Colored integrated absorption regions of NZCuB as example were calculated to evaluate ratios of B_3-units ($A(B_3)$) and B_4-units ($A(B_4)$) according to [3]. For the integration a linear baseline between minimum absorption at ~600 cm^{-1} and ~ 1600 cm^{-1} was used.

between 1160 cm^{-1}-1600 cm^{-1}, that features three maxima, at 1242 cm^{-1}, 1475 cm^{-1}, and the highest at 1367 cm^{-1} for LZB. The other broad region with also three maxima, at 887 cm^{-1}, 957 cm^{-1}, and 1047 cm^{-1}, is in the range 760 cm^{-1}-1160 cm^{-1} for LZB. It is remarkable, that the height ratios of the bands at ~1047 cm^{-1} and ~ 957 cm^{-1} change with composition. A further band occurs at 696 cm^{-1} and a cut band at 633 cm^{-1}.

The ratios of tetrahedral and trigonal borate units were calculated using the IR spectra as proposed by Möncke et al. [3]. Fig. 4 shows the integrated areas of the absorption $A(B_3)$ and $A(B_4)$ for NZCuB as an example. The integration was performed using the software Origin 2020 [45]. The absorption bands in the range (1135–1156 cm^{-1})-(1559–1580 cm^{-1}) were assigned to the stretching modes of B_3-units ($A(B_3)$) according to [3,26,27,32,33,36,52]. The bands in the range (758–778 cm^{-1})-(1135–1156 cm^{-1}) implied stretching modes of B_4-units ($A(B_4)$) [3,26,27,32,33,36,52]. The regions in the brackets denote the band shifts due to different network modifier or intermediate oxides.

Table 3 lists the calculated ratios of the areas assigned to tetrahedral $A(B_4)$ and trigonal $A(B_3)$ borate units of the glasses under study. The area $A(B_4)$ was divided by the relative absorption coefficients α (Zn) = 1.36 and α (Pb) = 1.5–1.0, as suggested by Möncke et al. [3]. The ratio $A(B_4)/A(B_3)$ spans a range between 0.53 and 0.79 for Pb and 0.53 and 0.65 for the other ones. This leads to N_4 between 0.34 and 0.44 for Pb as well as 0.35 and 0.39 for the others, respectively. The ratio $A(B_4)/A(B_3)$ decreases with increasing ionic radius in the row $Li^+ > Na^+ > K^+$. The ratio $A(B_4)/A(B_3)$ and N_4 of RZB are nearly similar to those of KZB. The ratio $A(B_4)/A(B_3)$ is higher for RZB1 with less Rb^+ ions and higher content of boron oxide than for RZB. The values for CaZB and LZB glass are almost similar. The ratio and N_4 decrease slightly in NZCuB in comparison to NZB.

Fig. 5 and Table S 2 in the supplemental material illustrate feasible deconvolutions of the normalized IR spectra and the resulting peak centers of LZB and RZB with a Gaussian alignment as also used in former studies [19,27,53] utilizing the software Origin 2020 [45].

The first band is cut off, but required for an appropriate fit according to [7,27]. The spectra of LZB and RZB seem to be comparable, but the deconvolutions emphasize differences. The bands 3–8 in the LZB spectrum are shifted to higher wavenumbers, and the bands 1 and 2 are shifted to lower wavenumbers in comparison to RZB. Bands 3 and 4 show large differences with respect to their amplitudes what explains the intensity changes of the IR spectra in the region of B_4 vibrations.

4. Discussion

4.1. Glass structure

Tables S 1 and S 2 (supplemental material) list the wavenumbers of the deconvoluted Raman und IR spectra of LZB and RZB. The assignments of Raman and IR bands were performed on the basis of the literature listed in Table 4 and will be discussed below.

Table 4 compiles the assigned structural units of the Raman and IR spectra of the glasses under study.

As known the bands of different borate units may appear in overlapping spectral regions. Thus, the assignments given in Table 4 and in the supplemental material for LZB and RZB need some consideration which will be started with the **Raman spectra**.

The assignment of the bands LZB (2) and RZB (2) to vibrations of Zn—O bonds is in accordance with the given references [17, 54, 55].

Metaborate units can be arranged in chains or rings [3,15,21,23,24,26,56]. Based on the results, given before, it is not possible to distinguish these units. Nevertheless, also four-coordinated $[B\emptyset_2O_2]^{3-}$ [26] or "loose" $[B\emptyset_4]^-$ tetrahedral groups [21,23,26] may contribute to the absorption in the region 345–680 cm^{-1} in addition to the metaborate units. The broad bands above 1250 cm^{-1} can also be assigned to metaborate groups. The bands at 679 cm^{-1} and 722 cm^{-1} in the LZB spectrum assigned to metaborate units are less intense relatively

Table 3
Ratio $A(B_4)/A(B_3)$ of the integrated IR absorption bands assigned to tetrahedral (B_4) and trigonal (B_3) borate units and the number of fourfold coordinated boron, $N_4 = A(B_4)/(A(B_4) + A(B_3))$. For the calculation the area $A(B_4)$ was divided by the relative absorption coefficients α (Zn) = 1.36 and α (Pb) = 1.5–1.0 according to [3].

Area Ratio	Unit	LZB	NZB	KZB	RZB	RZB1	LPbB	CaZB	NZCuB
$A(B_4)/A(B_3)$	[−]	0.65	0.58	0.55	0.56	0.60	0.53–0.79	0.64	0.53
$N_4 = A(B_4)/(A(B_4) + A(B_3))$	[−]	0.39	0.37	0.36	0.36	0.38	0.34–0.44	0.39	0.35

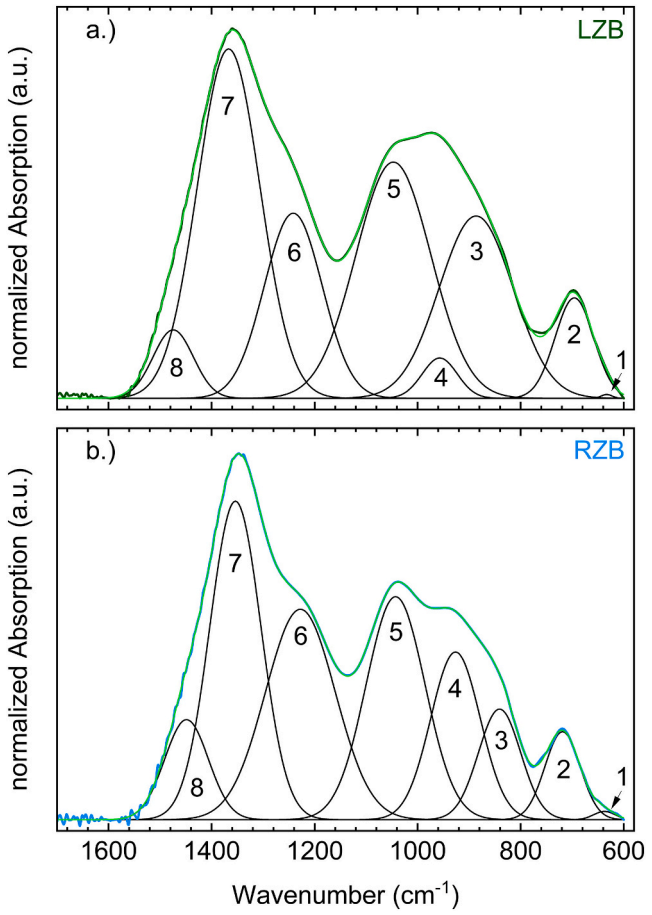

Fig. 5. Fit with Gauss alignment of the IR spectra of a.) LZB and b.) RZB obtained after transformation of ATR data, baseline correction and normalization. Bands are numbered consecutively. The correlation factor R^2 was 0.9998 for both fits.

and shift to higher wavenumbers with increasing ionic radius from Li^+ to Rb^+.

The pyroborate groups are doubtlessly recognizable by the bands between 840–850 cm^{-1} and 1180–1240 cm^{-1}, which do not overlap with other ones [3,21,23,24,26,33].

The large bands at around 770 cm^{-1} indicate six membered $BØ_3$-rings with one $[BØ_4]^-$-tetrahedron [3,21,30,33,57] or two $[BØ_4]^-$-tetrahedra [3,21,24,30,33]. That means, in both samples units like di-, tri-, tetra-, or pentaborate may be present. The large band at 775 cm^{-1} in the Raman spectrum of LZB is shifted to lower wavenumber, 767 cm^{-1} for RZB, with increasing alkali ion size. The same effect was observed by Chryssikos et al. [24] for binary alkali borate glasses ($0.17M_2O$-$0.83B_2O_3$, M = alkali ion).

The simultaneous presence of bands at 500 cm^{-1} (very broad), 667 cm^{-1}, 770 cm^{-1}, and 890 cm^{-1} was assigned to pentaborate [56–58]. The bands LZB (9), (12), (14), and (16) fit this pattern, the band LZB (10) was also assigned to pentaborate here referring to the described scatter of the band at around 500 cm^{-1} by Maniu et al. [58]. Since the bands (9) and (10) are missing in RZB, this group should not be part of the glass network of that sample.

The only open question is about the band at ~1050 cm^{-1} in RZB. Kamitsos et al. [23,26] assigned respective bands to carbonates CO_3^{2-} in alkali borate glasses with alkali contents ≥50 mol%. Even these are very weak. Hence, the band in RZB with an alkali content of ~19 mol% should not be caused by carbonates. Instead, the presence of diborates can explain this absorption. For diborates also bands at (490–570) cm^{-1} for isolated diborate, (930–950) cm^{-1}, (1035–1061) cm^{-1}, and (1120–1150) cm^{-1} are known [3,21,23,33,57,58]. Thus, the band at 970 cm^{-1} was assigned here to diborate possibly superimposed to metaborates. Bands between 490 cm^{-1} and 570 cm^{-1} are missing in RZB, hence, isolated diborates do not occur here.

To sum up the above discussion, the following statements can be made:

1. In LZB as well as in RZB metaborates, pyroborates, four-coordinated $[BØ_2O_2]^{3-}$, "loose" $[BØ_4]^-$ tetrahedral groups, and six membered $BØ_3$-rings with $[BØ_4]^-$-tetrahedra are detectable.
2. Pentaborate is present in LZB.
3. Diborate appears in RZB.

Finally, the spectra of the remaining glasses can be discussed. As shown in Fig. 1 and Fig. 2 the spectra of NZB, CaZB and NZCuB look alike LZB. Those of KZB and RZB1 are similar to RZB with respect to the presence or absence of bands in the region between (500–600) cm^{-1}.

The spectrum of LPbB differs from all the other ones in the region below 1100 cm^{-1}. The band at around ~290 cm^{-1} belongs to $[PbO_{4/2}]^{2-}$-units and the band at around 640 cm^{-1} is due to Pb-O-B bending vibrations as described by Ganguli and Rao [59]. The region between 690 cm^{-1} and 730 cm^{-1} indicates metaborate units and the region between 755 cm^{-1} and 775 cm^{-1} six membered $BØ_3$-rings with $[BØ_4]^-$-tetrahedra. Obviously, the metaborate band is significantly larger than that of the six membered $BØ_3$-rings with $[BØ_4]^-$-tetrahedra. The highest intensity at 1373 cm^{-1} is an additional indication of metaborate. The small but narrow band about 510 cm^{-1}, the overlapping band at ~(680–695) cm^{-1} and the band at ~(880–890) cm^{-1} can be interpreted as vibrations of pentaborate units. The bands in the region ~(840–950) cm^{-1} are due to presence of B_4 [21,24,26] and those between ~(950–1100) cm^{-1} belong to diborate units. This means, LPbB is the only sample, which contains pentaborate and diborate units simultaneously.

In the following the **IR spectra** shall be discussed. The IR spectra under discussion here can be subdivided into three regions:

- (600–800) cm^{-1}: overlapping bands of metaborate [3,27,33,60] and bending of B-O-B oxygen bridges [3,27,33,57,60].
- (800–1160) cm^{-1}: $[BØ_4]^-$-units belonging to different borate groups [3,27,33,60]. Based on the results of Raman spectroscopy, LZB and RZB differ concerning the presence of penta- and diborate groups, but both contain four-coordinated $[BØ_2O_2]^{3-}$ and "loose" $[BØ_4]^-$ tetrahedra. Despite this information it is not possible to assign the IR bands to those groups.
- (1160–1600) cm^{-1}: The assignment of band (6) and (7) to metaborate and pyroborate groups meets the results of Raman spectroscopy. At the highest wavenumbers, band (8), only vibrations of metaborate units are described in the literature [3,27,33,60]. Comparison of the spectra of LZB and RZB shows a downshift of the bands (6)–(8) with increasing ionic radius. According to Kamitsos et al. [27] this is an indication of the formation of diborate groups instead of pentaborate

Table 4
Characteristic bands given in the literature and assignments of Raman and infrared bands present in the spectra of LZB and RZB glass.

Structural units	Raman spectra	Reference	Assigned in	IR-spectra	Reference	Assigned in
	Wavenumber [cm^{-1}]			Wavenumber [cm^{-1}]		
Zn-O stretching vibrations and bending vibrations of O-Zn-O of ZnO_4 tetrahedra	250–300	[17,54,55]	LZB (2), RZB (2)	–		
four-coordinated $[BØ_2O_2]^{-3}$	345/350, 377/395, 680/ 675	[26]	LZB (4, 5, 6), RZB (4, 5, 6, 12)			
"loose" $[BØ_4]^-$ tetrahedra	370, 463, 1400–1600, 545, 900	[21,23,26]	LZB (8) RZB (8)			
pentaborate	~500, 660/667, 770, 785, 890/ 930	[56–58]	LZB (9, 10, 12, 16)			
metaborate $[BØ_2O]^-$-units in chains or rings	200–300 370, 463, 610–740, 1400–1600	[3,15,21,23,24,26,56]	LZB (0, 1, 2, 6, 7, 8, 11, 13, 18, 22, 23, 24) RZB (2, 3, 6, 7, 8, 11, 12, 13, 18, 22, 23, 24, 25)	1220–1260, 1400–1550, 1200–1650 738, 775, 500–650 (taken from crystalline metaborate) 1205, 1405	[3,27,33,60]	LZB (1, 6, 7, 8), RZB (1, 6, 7, 8)
six membered $BØ_3$-ring with one $[BØ_4]^-$-tetrahedron, (tri-, tetra-, or pentaborate groups)	770, 775, 780, 780–785, (770–785)	[3,21,30,33,57]	LZB (14)			
six membered $BØ_3$-ring with two $[BØ_4]^-$-tetrahedra, (triborate, diborate, di-tri- or di-pentaborate groups)	755, 760, 765, 770 (755–770)	[3,21,24,30,33]	RZB (14)			
B-O-B bending vibrations				600–800, 710, 720, 765, 690–730, 760–770, 550–800, 700 (deformation modes)	[3,27,33,57,60]	LZB (2), RZB (2)
$[BØ_4]^-$-units in etc. tri, tetra-, pentaborate, diborate, di-tri- or di-pentaborate groups	500, 535, 900, 945	[21,24,26]	LZB (14, 17) RZB (14, 17)	800–1200, 800–1100, 1050, 880 960, 1040	[3,27,33,60]	LZB (3, 4, 5) RZB (3, 4, 5)
pyroborate units	810, 820, 830, 850, 1180, 1240, 1210, 1220	[3,21,23,24,26,33]	LZB (15, 20, 21), RZB (15, 21)	1120–1140, 1225–1270, 1150–1300 1200–1350, 1365	[3,27,33]	LZB (6, 7) RZB (6, 7)
B–O stretching modes of diborate units	490–570 (isolated diborate), 500, 950, 1150, 1120 1050–1061	[3,21,23,33,57,58]	RZB (18, 19)	675, 785, ~1000, 970, 960, 880, 1060 900–1000, 850, 935, 1040	[3,27,33]	RZB (3, 4, 5)

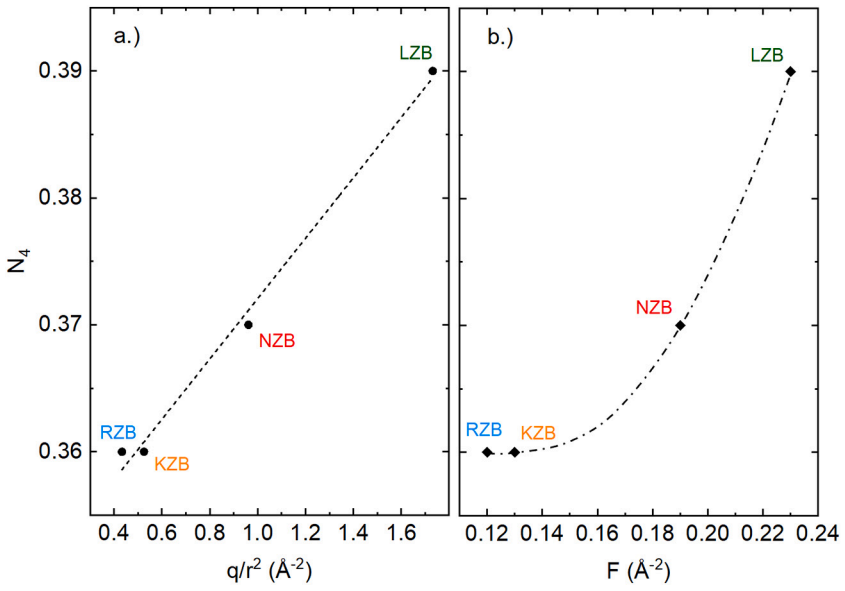

Fig. 6. B_4-content, N_4, as a function of a.) field strength of the modifying cation, q/r^2 [31], where q is the formal charge and r is the ionic radius taken from [48] and b.) Dietzel field strength [50]. The straight line in a.) belongs to a linear fit, the line in b.) serves as guide for the eyes.

groups. Hence, the IR spectra support the results of the Raman spectra.

The IR spectra strengthen the interpretation of simultaneous presence of penta- and diborate groups in LPbB given above. The spectra in the region of the $[B\emptyset_4]^-$-units are similar with respect to the intensity ratios of the bands at 957 cm^{-1} and 1047 cm^{-1} for LZB and LPbB. Otherwise, the bands of B_3-units of LPbB are shifted analogously as those of RZB.

An important contribution of the IR spectra is given by the possibility to estimate the relative amounts of B_3 and B_4-units as listed in Table 3. The ratios and thus the numbers of B_4-units decrease from $Li^+ < Na^+ < K^+$ with increasing ionic radius. In binary alkali borate glasses Zhong and Bray [22], Kamitsos [35] as well as Chryssikos et al. [24] found a higher number of NBOs and B_3, but less B_4-units with increasing ionic size, similar to the trend in the alkali zinc borate glasses here. The results of the more precise NMR spectroscopic determination of N_4 values in binary alkali borate glasses indicate, that the difference between K^+ and Rb^+ is low [22]. This is also observed in the data given in Table 3. This means for glasses with almost equal alkali contents, that the ratio of Rb^+ ions forming B_4 is comparable to this of K^+ but lower than the ratios of Li^+ and Na^+. The comparison of the relative amounts of B_4 units of the samples RZB and RZB1 supports this interpretation. The Rb-content of RZB1 seems to be close to the maximum of N_4 formation and further addition of Rb_2O (RZB) results in the formation of NBO and thus decrease of B_4.

Fig. 6 a.) indicates a linear trend of the B_4-content as a function of field strength of the alkali ion, q/r^2 [31], where q is the formal charge and r is the ionic radius taken from [48]. Chryssikos et al. [31] described also a linear trend of B_4-content for alkaline earth ions Ba^{2+} to Ca^{2+}, but in the opposite direction decreasing with increasing field strength. The B_4-content as a function of the Dietzel field strength of the alkali ions exhibits a curved trend.

According to the Lewis acid-base concept it was found, that Li^+ acts as a hard acid, promoting B_4-units as a hard base [24,35,61]. Vice versa larger alkali ions are softer acids promoting formation of NBOs and B_3-units as a softer base [24,35,61]. Additional to the acid-base concept and the ion size, the alkali ions differ in their Dietzel field strength - decreasing from Li to Rb, in their polarizability - increasing from Li to Rb and in the steric effects because of increasing size [24]. The combination of these alkali properties (and the acid-base behavior) decides, to which side the equilibrium is shifted in eq. (3) [24,26].

$$[B\emptyset_4]^- \rightleftarrows [B\emptyset_2O]^- \quad (3)$$

It is remarkable, that the relative amounts of B_4 units in LZB and CaZB are matchable what underlines the similarity of the glass structures found by Raman spectroscopy. Another observation concerns the effect of partial substitution of Zn by Cu, which leads to a decrease of B_4 units.

Due to the fact that the relative absorption coefficient α of Pb containing glasses cannot exactly be given (see [3]) only a rough estimation of the B_4-percentage is possible. The minimum and maximum values obtained here, comprise the hole range computed for all the other glasses under consideration.

Summarizing the results of Raman and IR spectra the **function of the ions** in the networks can be described as follows:

1. Alkali ions preferably form B_4 groups and to a lesser extent NBOs. With increasing ionic radius, the ability to form B_4 decreases. As a consequence, LZB and NZB are able to form pentaborate whereas the networks of KZB and RZB do not contain this group. Certain percentages of alkali ions contribute to the formation of metaborates. Hence, the respective bands are shifted.
2. Zinc ions favorably compensate the NBOs of pyroborates. This explains the similar absorption bands (15) in LZB and RZB. The bands LZB (2) and RZB (2) indicate formation of ZnO_4 tetrahedra, which were also described by other authors [17,54,55].
3. The similarity of the Raman and IR spectra of CaZB and LZB hints to formation of comparable borate networks.
4. The substitution of Zn^{2+} by Pb^{2+} results in the simultaneous formation of penta- and diborate groups, which was not observed in any other sample.
5. It can be expected, that the substitution of Zn^{2+} by Cu^{2+} leads to an increase of NBOs [15]. Due to the small copper content the spectra are not that different, that a comprehensive discussion is possible here.

4.2. Relations between glass composition, structure, and properties

The differences between measured and calculated properties collected in Table 2 point out, that the data in the SciGlass database [46] are not sufficient to predict the properties of the glasses under study here. Since zinc borate glasses could become more important in future technologies, it is necessary to fill the lack of data.

The maximum deviation between measured and calculated **density** of about 7% strengthens the lack of data regarding the glasses under study in SciGlass [46]. As shown in Fig. 7 a.) the samples with alkali ions Li^+, Na^+, and K^+ indicate a decreasing density and **APD** with increasing ionic radius and molar mass M.

Since the ionic radii of K^+ and Rb^+ have only small difference (see Table 2), the effect of the higher molar mass of Rb is almost compensated leading to almost similar APD of those samples.

The decrease in APD from Li^+ to K^+ due to the larger alkali size

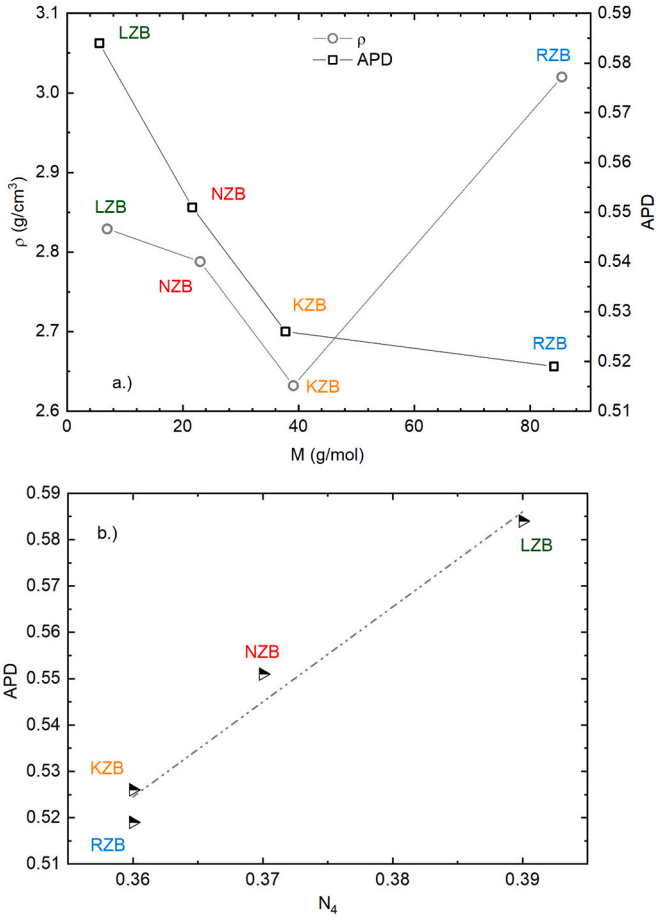

Fig. 7. a.) Glass density and atomic packing density APD as functions of the molar mass M of the alkali ions and b.) APD as function of N_4. The lines in a.) provide guidelines for the eyes and in b.) a linear trend.

explains the decrease of glass density. Rb^+ exhibits the highest density. Feller et al. [62,63] also showed, that Rb borate glasses have a higher density than Li, Na and K borate glasses. Rb leads to higher density due to its more than doubled mass of 85.468 g/mol [64] in comparison to 39.098 g/mol for K [64]. A comparable density to those measured here of about 2.8 g/cm^3 for xNa_2O-27ZnO-(100-x)B_2O_3 was published by Gowda and Anavekar [18].

The density of CaZB is 0.31 g/cm^3 higher than the density 2.79 g/cm^3 of 50CaO-50B_2O_3 glass [63]. This can be explained by the higher mass of Zn^{2+} compared to that of Ca^{2+}.

The substitution of Zn^{2+} with Pb^{2+} leads to higher density of LPbB than of LZB due to higher mass of Pb^{2+}, see Table 2. Ganguli and Rao [59] found similar densities for (30,20)Li_2O-20PbO-(50,60)B_2O_3, respectively.

The small deviation of ρ due to the substitution of Zn^{2+} by Cu^{2+} shows a slight decrease of ρ, Table 2. Yao et al. [15] found a slight decrease in the density of zinc borate glasses with the addition of (1−10) mol% CuO.

Consideration of **molar volume and APD** allows gaining a deeper insight into the relations to spectroscopically determined structural units.

The molar volume will be as smaller as closer the constituents of the glassy network are packed. Vice versa, the APD will become higher. Due to this complementarity of information from both properties in the following the discussion will only deal with APD. Concerning borate glasses, it is known, that APD becomes higher when B_4-groups are formed instead of B_3-groups. This trend is shown in Fig. 7 b.) for the glasses under study. Such a relation was described e.g. by Giri et al. [65]. They found a maximum of APD in xLi_2O-(100-x)B_2O_3 glasses at x = 0.4 being the composition with the maximum fraction of B_4-units. Additionally, these authors divided the glasses depending on the alkali ions present into two groups: (i) glasses with r(alkali) > r(O), i.e. containing K^+, Rb^+ and Cs^+, show ionic packing and (ii) Li- and Na-borate glasses, where r(M) < r(O) holds, are characterized by a covalent packing dominated by oxygen [65]. The distinction of two groups of alkali cations as done by Giri et al. [65] is similar to the subdivision defined when utilizing the Raman spectra.

APD of CaZB is close to that of LZB and the respective ratios N_4 are equal again showing the relationship between packing density and number of B_4-units.

The APD of LPbB is between those of KZB and NZB, but lower than that of LZB, see Table 2. This effect can not only be explained by the number N_4. Additionally, the ionic radius of Pb^{2+}, that is nearly 5/3 of the radius of Zn^{2+}, when both in fourfold coordination, is responsible for the lower APD of LPbB compared to LZB.

Due to the substitution of Zn^{2+} by Cu^{2+} a slight decrease of APD was observed. Since the radii of Zn^{2+} and Cu^{2+} in fourfold coordination are similar, the glass structure and thus the slightly smaller ratio of N_4 for NZCuB than for NZB in Table 3 explains the smaller APD.

The differences between the **glass transition temperatures** measured by means of dilatometry and DTA, respectively, lie in the measurement uncertainty of ±5 °C. Fig. 8 shows a plot of transition temperatures vs. the B_4-content of the glasses determined by IR spectroscopy. As shown in Fig. 6 N_4 increases with decreasing ionic radius of the alkali cations. Thus, respective plots can be discussed in the same manner. The tendency of decreasing T_g with increasing ionic radius of the alkali ions was in former studies explained by Chryssikos et al. [24,31] in binary alkali borate glasses. They explained the decrease in T_g with increasing ionic radii to the increasing number of NBOs [24,31]. An increase of non-bridging oxygens with ionic radius is synonymous with a decrease of B_4-content in the glasses under study here.

The collected data in [31] show similar transition temperatures for up to x = 20 in x(Li/Na)$_2$O-80B_2O_3, comparable to the values found for the ~20(Li/Na)$_2$O-27ZnO-53B_2O_3 glasses here. Since the Zn-content in the alkali zinc borate glasses is constant, Zn^{2+} does not influence this trend, but leads to higher values of T_g in comparison to the 20(Li/Na)$_2$O-80B_2O_3 glasses [31,66]. This can be explained by the fact, that zinc can on the one hand weaken the network by formation of NBOs and on the other hand strengthen it by formation of ZnO_4-groups.

As also found by Chryssikos et al. [31] for diborates, the number of B_4-units in calcium diborates or in case here the ratio N_4 of CaZB given in Table 3 is lower or similar than for lithium diborates or LZB respectively, but T_g is (100–150) °C higher. This effect is explained in [31,67] by the higher "crosslinking" potential of Ca^{2+} due to its higher coordination number.

Pb^{2+} in LPbB instead of Zn^{2+} in LZB results in lower T_g. A similar trend is found in 50PbO-50B_2O_3, T_g = 396 °C, and 50ZnO-50B_2O_3, T_g = 571 °C, described by Yao et al. [15]. For 0.2PbO-0.3Li_2O-0.5B_2O_3 Ganguli and Rao [59] measured a T_g of 387 °C, which fits well to the here measured T_g.

The substitution of Zn^{2+} in NZB by Cu^{2+} in NZCuB leads to a small decrease in T_g effected by the decrease in the ratios N_4 shown in Table 3. In Yao et al. [15] the decrease of T_g was attributed to the higher coordination number of Cu^{2+} acting as network modifier in an octahedral coordination.

The increase of the **coefficient of thermal expansion** in the row Li^+ < Na^+ < K^+ < Rb^+ can be explained by combined reasons: (i) the decrease of the field strength of the cations [50], (ii) decrease of B_4-content, and vice versa increase of NBO content as described by Shelby [66] and Chryssikos et al. [24]. Since KZB and RZB have similar B_4-contents, the difference between their CTEs shows the influence of cation field strength.

Since 50ZnO-50B_2O_3 glass has a low CTE of 5.2 10^{-6} K^{-1} [15], zinc seems to rarely impact the CTE and the dependence of CTE on the alkali ions is significantly enhanced. The substitution of Zn^{2+} in LZB by Pb^{2+} in LPbB leads to an increase of the CTE due to lower filed strength q/r^2 [16] and higher polarizability of Pb^{2+} [68]. Since the field strength q/r^2 of Ca^{2+} is higher than that of the alkali ions shown in Table 2, the CTE of CaZB is lower than the CTE of the alkali zinc borate glasses. As found for ZnO-CuO-B_2O_3 glasses in [15], the substitution of Zn^{2+} by Cu^{2+} had no significant influence on the CTE of NZCuB, since the ionic radii of Zn^{2+} and Cu^{2+} are similar.

Rouxel [47] found a proportionality between **Young's Modulus** E and APD. The strong decrease of E with decreasing APD from Li^+ to Rb^+, as shown in Fig. 9, fits well to Rouxel's findings [47]. Additionally, the single-bond strengths of Me-O (Me = Li, Na, K, Rb) are diminishing from Li^+ (36 kcal [69]) to Rb^+ (12 kcal [69]). Taking both aspects into account, the decrease of E is stronger than calculated by SciGlass [46].

The theory of Rouxel [47] additionally explains: (i) the decreasing E from LZB to LPbB, 92.5 GPa to 74.6 GPa, with the decrease of APD from

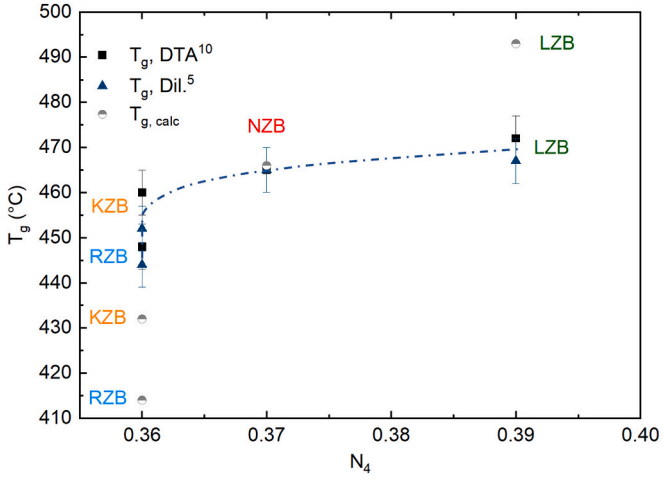

Fig. 8. Transition temperature, T_g, measured by means of DTA and dilatometer, as functions of N_4. For comparison, T_g, calculated by SciGlass [46] is shown. The dashed line is a guideline for the eyes.

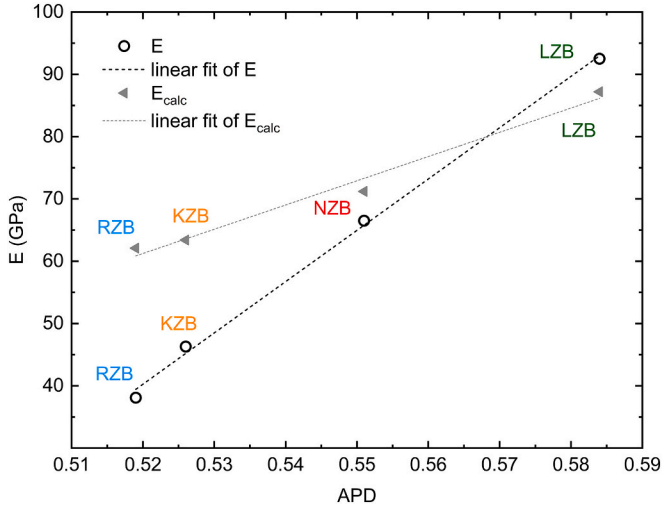

Fig. 9. Measured and calculated Young's Modulus as function of APD. The dashed lines are linear fits. Measurement uncertainty is not larger than the symbols.

0.584 to 0.528; while the single-bond strengths of Zn—O and Pb—O are similar (36 kcal if modifiers and ~ 73 kcal if intermediates [69]) and (ii) the decreasing E from NZB to NZCuB, 66.5 GPa to 65.3 GPa, with the decrease of APD from 0.551 to 0.540. Yao et al. [15] suggested, that the small decrease of elastic moduli in ZnO-xCuO-B_2O_3 by the substitution of Zn^{2+} by Cu^{2+} is caused by the decrease in APD, since the single-bond strength of Zn—O and Cu—O are similar. That effect occurs in NZB and NZCuB, as shown above.

Since CaZB has a lower APD than LZB, the "crosslinking" ability of Ca^{2+}, mentioned above, explains the higher E compared to LZB.

Only three samples had the sufficient size to determine the **shear modulus** and the **Poisson's ratio** here. Their values fit to those of other sodium borate glasses, calculated from the data of Makishima and Mackenzie [47,70].

5. Conclusion

Despite the complexity of ternary composition with regard to the competitive role of network modifier and intermediate oxide, conclusions in terms of structure, e.g., the occurrence of specific borate groups, were deduced from the combination of Raman- and IR-spectroscopies. The type of alkali ion is in charge of the kind of formed B_4 containing borate groups. Thus, the glasses under study were divided into two groups in view of the appearance of pentaborate in LZB, NZB, NZCuB and CaZB or diborate in KZB, RZB, RZB1. In LPbB, both penta- and diborate groups, provide the B_4-content. The here shown results indicate, that the alkali ions mainly form B_4-units and zinc ions preferably compensate NBOs in the glasses under study.

K^+ and Rb^+ containing zinc borate glasses are similar in B_4-content, N_4, here. In the alkali series N_4 decreases linearly with the field strength q/r^2. Correspondingly, the properties atomic packing density, T_g, and Young's Modulus show a decrease with decreasing N_4 in the row $Li^+ > Na^+ > K^+ > Rb^+$. An opposite trend is indicated by the CTE, that increases with decreasing N_4 and field strength.

The N_4 of Ca^{2+}-glass is equal to that of Li^+-glass underlining the formation of similar borate units. Additionally, the APD is close to that of Li^+-glass. In spite of N_4 and APD similar to Li^+-glass, the Ca^{2+}- glass exhibits higher T_g and Young's Modulus because of the higher "crosslinking" potential due to its higher coordination number of Ca^{2+} [33,70]. The CTE of Ca^{2+}-glass is lower than that of the alkali glasses concerning the higher field strength of Ca^{2+}.

Substitution of Zn^{2+} with Pb^{2+} in alkali containing borate glasses leads to lower T_g, lower APD, thus lower Young's Modulus. Due to the not exactly known relative absorption coefficient of B_4 of Pb containing glasses the respective N_4 values cover a range of 0.34–0.44. The CTE of Pb - compared to the Zn containing glasses - increases due to decreasing filed strength q/r^2 [16] and higher polarizability of Pb^{2+} [68]. The increase in density of glasses with Pb^{2+} instead of Zn^{2+} occurs because of the higher molar mass of lead.

The replacement of 18.5% of the total Zn^{2+}-amount by Cu^{2+} results in a slight decrease of N_4. This causes a smaller APD and thus smaller Young's Modulus of the Cu^{2+} containing glass under study. However, the differences in properties are slight.

The new property data of the glasses under study expand the data pool for zinc borate glasses. The large differences between measured and with SciGlass [46] calculated properties documented here underline the necessity to gain experimental data. Hence, further variation of the composition including the alkali/zinc ratio is required to fill the lack of data regarding ternary alkali zinc borate glasses and to fully understand their structure.

Data availability statement

The data that support the findings of this study are available from the corresponding authors upon reasonable request.

CRediT authorship contribution statement

Lina Heuser: Conceptualization, Data curation, Formal analysis, Investigation, Methodology, Visualization, Writing – original draft, Writing – review & editing. **Marianne Nofz:** Conceptualization, Supervision, Visualization, Writing – original draft, Writing – review & editing.

Declaration of Competing Interest

The authors declare that they have no known competing financial interests or personal relationships that could have appeared to influence the work reported in this paper.

Acknowledgement

The financial support of the Deutsche Forschungsgemeinschaft (DFG) via MU 963/17-1 is gratefully acknowledged. The authors sincerely thank A. Marek and S. Rüster for sample preparation, A. Kohl for IR measurements, and T. Schmid for support in Raman spectroscopy.

Appendix A. Supplemental data

In the supplemental material two figures showing the raw Raman and IR-spectra as well as two tables containing single band assignments are given. The supplemental data can be found online at https://doi.org/10.1016/j.nocx.2022.100109.

References

[1] N.H. Afrizal, N. Yahya, N.M. Yusoff, A. Kasim, A. Hashim, Physical, mechanical and structural properties of Yttrium oxide doped zinc borate glasses, Solid State Phenom. 307 (2020) 327–335, https://doi.org/10.4028/www.scientific.net/SSP.307.327.

[2] N.M. Bobkova, S.A. Khot'ko, Structure of zinc-borate low-melting glasses derived from IR spectroscopy data, J. Appl. Spectrosc. 72 (6) (2005) 853–857, https://doi.org/10.1007/s10812-006-0015-2.

[3] D. Möncke, E.I. Kamitsos, D. Palles, R. Limbach, A. Winterstein-Beckmann, T. Honma, Z. Yao, T. Rouxel, L. Wondraczek, Transition and post-transition metal ions in borate glasses: borate ligand speciation, cluster formation, and their effect on glass transition and mechanical properties, J. Chem. Phys. 145 (12) (2016), 124501, https://doi.org/10.1063/1.4962323.

[4] D. Ehrt, Structure, properties and applications of borate glasses, Glass Technol. 41 (6) (2000) 182–185.

[5] D. Ehrt, Zinc and manganese borate glasses–phase separation, crystallisation, photoluminescence and structure, Phys. Chem. Glasses Eur. J. Glass Sci. Technol. B 54 (2) (2013) 65–75.

[6] C. Gautam, A.K. Yadav, A.K. Singh, A review on infrared spectroscopy of borate glasses with effects of different additives, ISRN Ceram. 2012 (2012), https://doi.org/10.5402/2012/428497.

[7] A. Saidu, H. Wagiran, M.A. Saeed, Y.S.M. Alajerami, Structural properties of zinc lithium borate glass, Opt. Spectrosc. 117 (3) (2014) 396–400, https://doi.org/10.1134/S0030400x14090239.

[8] M. Eberstein, U. Schmidt, S. Korner, K. Reinhardt, R. Jurk, U. Partsch, In-situ observations of glass frit related effects during the front side paste contact formation, in: A. Derek (Ed.), 2014 IEEE 40th Photovoltaic Specialist Conference (PVSC), IEEE, Denver, USA, 2014, pp. 3463–3469.

[9] S. Körner, M. Eberstein, WO 2016/062820 A1, Method for Producing a Silver-Containing Glass Powder, and Use of the Glass Powder, Fraunhofer-Gesellschaft zur Förderung der angewandten Forschung, 2016.

[10] S. Körner, Lösungs-und Ausscheidungsprozesse in silberhaltigen Glasschmelzen bei der thermischen Kontaktierung von multikristallinem Silicium, Technische Universität Dresden, 2018.

[11] A. Sayyadi-Shahraki, E. Taheri-Nassaj, S.A. Hassanzadeh-Tabrizi, H. Barzegar-Bafrooei, Low temperature cofirable $Li_2Zn_3Ti_4O_{12}$ microwave dielectric ceramic with Li_2O-ZnO-B_2O_3 glass additive, J. Mater. Sci. Mater. Electron. 25 (1) (2014) 355–360, https://doi.org/10.1007/s10854-013-1594-3.

[12] G. Chen, M. Hou, Y. Bao, C. Yuan, C. Zhou, H. Xu, Silver co-firable $Li_2ZnTi_3O_8$ microwave dielectric ceramics with LZB glass additive and TiO_2 dopant, Int. J. Appl. Ceram. Technol. 10 (3) (2013) 492–501, https://doi.org/10.1111/j.1744-7402.2012.02754.x.

[13] S.S. Danewalia, K. Singh, S.K. Arya, Influence of vanadium oxide on non-isothermal crystallization kinetics of zinc lithium borate glasses, J. Non-Cryst. Solids 553 (2021), 120471, https://doi.org/10.1016/j.jnoncrysol.2020.120471.

[14] A. Kannappan, S. Thirumaran, R. Palani, Elastic and mechanical properties of glass specimen by ultrasonic method, ARPN J. Eng. Appl. Sci 4 (1) (2009) 27–31.

[15] Z.Y. Yao, D. Möncke, E.I. Kamitsos, P. Houizot, F. Célarié, T. Rouxel, L. Wondraczek, Structure and mechanical properties of copper-lead and copper-zinc borate glasses, J. Non-Cryst. Solids 435 (2016) 55–68, https://doi.org/10.1016/j.jnoncrysol.2015.12.005.

[16] N.M. Bobkova, S.A. Khot'ko, Zinc oxide in borate glass-forming systems, Glas. Ceram. 62 (5–6) (2005) 167–170, https://doi.org/10.1007/s10717-005-0064-7.

[17] M. Bettinelli, A. Speghini, M. Ferrari, M. Montagna, Spectroscopic investigation of zinc borate glasses doped with trivalent europium ions, J. Non-Cryst. Solids 201 (3) (1996) 211–221, https://doi.org/10.1016/0022-3093(96)00134-2.

[18] V.C.V. Gowda, R.V. Anavekar, Elastic properties and spectroscopic studies of Na_2O-ZnO-B_2O_3 glass system, Bull. Mater. Sci. 27 (2) (2004) 199–205, https://doi.org/10.1007/Bf02708505.

[19] M.S. Gaafar, N.S. Abd El-Aal, O.W. Gerges, G. El-Amir, Elastic properties and structural studies on some zinc-borate glasses derived from ultrasonic, FT-IR and X-ray techniques, J. Alloy. Compd. 475 (1-2) (2009) 535–542, https://doi.org/10.1016/j.jallcom.2008.07.114.

[20] J. Krogh-Moe, The infrared spectra and the structure of some anhydrous zinc borates, Z. für Kristallogr. 117 (2–3) (1962) 166–170, https://doi.org/10.1524/zkri.1962.117.2-3.166.

[21] W.L. Konijnendijk, J.M. Stevels, The structure of borate glasses studied by Raman scattering, J. Non-Cryst. Solids 18 (3) (1975) 307–331.

[22] J. Zhong, P.J. Bray, Change in boron coordination in alkali borate glasses, and mixed alkali effects, as elucidated by NMR, J. Non-Cryst. Solids 111 (1) (1989) 67–76, https://doi.org/10.1016/0022-3093(89)90425-0.

[23] E.I. Kamitsos, M.A. Karakassides, G.D. Chryssikos, Structure of borate glasses. Part 1. Raman-study of cesium, rubidium, and potassium borate glasses, Phys. Chem. Glasses 30 (6) (1989) 229–234.

[24] G.D. Chryssikos, E.I. Kamitsos, M.A. Karakassides, Structure of borate glasses. Part 2. Alkali induced network modifications in terms of structure and properties, Phys. Chem. Glasses 31 (3) (1990) 109–116.

[25] E. Kamitsos, A. Patsis, G.D. Chryssikos, Infrared reflectance investigation of alkali diborate glasses, J. Non-Cryst. Solids 152 (2–3) (1993) 246–257, https://doi.org/10.1016/0022-3093(93)90258-Y.

[26] E.I. Kamitsos, G.D. Chryssikos, Borate glass structure by Raman and infrared spectroscopies, J. Mol. Struct. 247 (1991) 1–16, https://doi.org/10.1016/0022-2860(91)87058-P.

[27] E.I. Kamitsos, A.P. Patsis, M.A. Karakassides, G.D. Chryssikos, Infrared reflectance spectra of lithium borate glasses, J. Non-Cryst. Solids 126 (1–2) (1990) 52–67, https://doi.org/10.1016/0022-3093(90)91023-K.

[28] J.F. Stebbins, S.E. Ellsworth, Temperature effects on structure and dynamics in borate and borosilicate liquids: high-resolution and high-temperature NMR results, J. Am. Ceram. Soc. 79 (9) (1996) 2247–2256, https://doi.org/10.1111/j.1151-2916.1996.tb08969.x.

[29] S. Kroeker, J.F. Stebbins, Three-coordinated Boron-11 chemical shifts in borates, Inorg. Chem. 40 (24) (2001) 6239–6246, https://doi.org/10.1021/ic010305u.

[30] T.W. Bril, Raman Spectroscopy of Crystalline and Vitreous Borates, Chemical Engineering and Chemistry, Technische Hogeschool Eindhoven, Eindhoven, 1976.

[31] G.D. Chryssikos, E.I. Kamitsos, Y.D. Yiannopoulos, Towards a structural interpretation of fragility and decoupling trends in borate systems, J. Non-Cryst. Solids 196 (1996) 244–248, https://doi.org/10.1016/0022-3093(95)00594-3.

[32] E.I. Kamitsos, M.A. Karakassides, G.D. Chryssikos, A vibrational study of lithium sulfate based fast ionic conducting borate glasses, J. Phys. Chem. 90 (19) (1986) 4528–4533, https://doi.org/10.1021/j100410a010.

[33] E.I. Kamitsos, M.A. Karakassides, G.D. Chryssikos, Vibrational spectra of magnesium-sodium-borate glasses. 2. Raman and mid-infrared investigation of the network structure, J. Phys. Chem. 91 (5) (1987) 1073–1079, https://doi.org/10.1021/j100289a014.

[34] E.I. Kamitsos, M.A. Karakassides, G.D. Chryssikos, Far-infrared spectra of binary alkali borate glasses, Solid State Ionics 28 (1988) 687–692, https://doi.org/10.1016/S0167-2738(88)80126-7.

[35] E.I. Kamitsos, Modifying role of alkali-metal cations in borate glass networks, J. Phys. Chem. 93 (4) (1989) 1604–1611, https://doi.org/10.1021/j100341a083.

[36] E.I. Kamitsos, Y.D. Yiannopoulos, C.P. Varsamis, H. Jain, Structure-property correlation in glasses by infrared reflectance spectroscopy, J. Non-Cryst. Solids 222 (1997) 59–68, https://doi.org/10.1016/S0022-3093(97)90097-1.

[37] J. Krogh-Moe, On the Structure of Boron Oxide and Alkali Borate Glasses, Almqvist & Wiksell, Uppsala, 1959.

[38] J. Krogh-Moe, The structure of vitreous and liquid boron oxide, J. Non-Cryst. Solids 1 (4) (1969) 269–284, https://doi.org/10.1016/0022-3093(69)90025-8.

[39] D.L. Griscom, Borate glass structure, in: L.D. Pye, V.D. Frechette, N.J. Kreidl (Eds.), Borate Glasses Structure, Properties, Applications, Materials Science Research vol. 12, Plenum Press, New York and London, 1978, pp. 11–138.

[40] A. Kajinami, Y. Harada, S. Inoue, S. Deki, N. Umesaki, The structural analysis of zinc borate glass by laboratory EXAFS and X-ray diffraction measurements, Jpn. J. Appl. Phys. 38 (S1) (1999) 132–135, https://doi.org/10.7567/Jjaps.38s1.132.

[41] Deutsches Institut für Normung e.V.. DIN 51086-2, Prüfung von oxidischen Roh-- und Werkstoffen für Keramik, Glas und Glasuren - Teil 2: Bestimmung von Ag, As, B, Ba, Be, Bi, Ca, Cd, Ce, Co, Cr, Cu, Er, Eu, Fe, La, Mg, Mn, Mo, Nd, Ni, P, Pb, Pr, S, Sb, Se, Sn, Sr, Ti, V, W, Y, Yb, Zn, Zr durch optische Emissionsspektrometrie mit induktiv gekoppeltem Plasma (ICP OES), Berlin, 2004.

[42] O.V. Mazurin, Y.V. Gankin, Glass transition temperature: problems of measurement procedures, Glass Technol.-Part A 49 (5) (2008) 229–233.

[43] ASTM International, ASTM E1876–15, Standard Test Method for Dynamic Young's Modulus, Shear Modulus, and Poisson's Ratio by Impulse Excitation of Vibration, West Conshohocken, PA, USA, 2015.

[44] X. Wang, X.-g. Fan, Y.-j. Xu, X.-f. Wang, H. He, Y. Zuo, A baseline correction algorithm for Raman spectroscopy by adaptive knots B-spline, Meas. Sci. Technol. 26 (11) (2015) 115503 (7pp), https://doi.org/10.1088/0957-0233/26/11/115503.

[45] OriginLab Corporation, Origin, Version 2020, Northampton, MA, USA, 2020.

[46] O.V. Mazurin (Ed.), SciGlass 6.5: Glass Information System-Glass Property Database, Institute of Theoretical Chemistry ITC Inc., Newton, USA, 2005.

[47] T. Rouxel, Elastic properties and short-to medium-range order in glasses, J. Am. Ceram. Soc. 90 (10) (2007) 3019–3039, https://doi.org/10.1111/j.1551-2916.2007.01945.x.

[48] R.D. Shannon, Revised effective ionic-radii and systematic studies of interatomic distances in halides and chalcogenides, Acta Cryst. A 32 (5) (1976) 751–767, https://doi.org/10.1107/S0567739476001551.

[49] T. Welter, U. Marzok, J. Deubener, S. Reinsch, R. Müller, Hydrogen diffusivity in sodium aluminosilicate glasses, J. Non-Cryst. Solids 521 (2019), 119502, https://doi.org/10.1016/j.jnoncrysol.2019.119502.

[50] H. Scholze, Glass – Nature, Structure and Properties, Springer, New York, Berlin, Heidelberg, 1991.

[51] T. Schmid, R. Jungnickel, P. Dariz, Raman band widths of anhydrite II reveal the burning history of high-fired medieval gypsum mortars, J. Raman Spectrosc. 50 (8) (2019) 1154–1168, https://doi.org/10.1002/jrs.5632.

[52] U. Selvaraj, K.J. Rao, Infrared spectroscopic study of mixed-alkali effect in borate glasses, Spectrochim. Acta A 40 (11−12) (1984) 1081–1085, https://doi.org/10.1016/0584-8539(84)80137-3.

[53] Y.M. Moustafa, H. Doweidar, G. El-Damrawi, Utilisation of infrared spectroscopy to determine the fraction of the four coordinated borons in borate glasses, Phys. Chem. Glasses 35 (2) (1994) 104–106.

[54] E.R. Lippincott, J.A. Psellos, M.C. Tobin, The Raman spectra and structures of aluminate and zincate ions, J. Chem. Phys. 20 (3) (1952) 536, https://doi.org/10.1063/1.1700478.

[55] A.K. Yadav, P. Singh, A review of the structures of oxide glasses by Raman spectroscopy, RSC Adv. 5 (83) (2015) 67583–67609, https://doi.org/10.1039/c5ra13043c.

[56] G. Padmaja, P. Kistaiah, Infrared and Raman spectroscopic studies on alkali borate glasses: evidence of mixed alkali effect, J. Phys. Chem. A 113 (11) (2009) 2397–2404, https://doi.org/10.1021/jp809318e.

[57] W.L. Konijnendijk, The Struture of Borosilicate Glasses, Philips Res. Repts Suppl. 1975, No. 1, Technische Hogeschool Eindhoven, Eindhoven, 1975.

[58] D. Maniu, T. Iliescu, I. Ardelean, S. Cinta-Pinzaru, N. Tarcea, W. Kiefer, Raman study on B_2O_3-CaO glasses, J. Mol. Struct. 651 (2003) 485–488, https://doi.org/10.1016/S0022-2860(03)00129-7.

[59] M. Ganguli, K.J. Rao, Structural role of PbO in Li_2O-PbO-B_2O_3 glasses, J. Solid State Chem. 145 (1) (1999) 65–76, https://doi.org/10.1006/jssc.1999.8221.

[60] E.I. Kamitsos, Infrared studies of borate glasses, Phys. Chem. Glasses 44 (2) (2003) 79–87.

[61] N. Uchida, T. Maekawa, T. Yokokawa, Hard basicity of borate anion clusters, J. Non-Cryst. Solids 88 (1) (1986) 1–10, https://doi.org/10.1016/S0022-3093(86)80083-7.

[62] S. Feller, S. Nijhawan, M. Royle, J. MacKenzie, J. Taylor, M. Sharma, E.I. Kamitsos, G.D. Chryssikos, A.P. Patsis, P.J. Bray, Physical properties and spectroscopy of rubidium and caesium borate glasses with exceptionally high alkali content, Chim. Chronica, New Series 23 (1994) 309–314.

[63] N.P. Lower, J.L. McRae, H.A. Feller, A.R. Betzen, S. Kapoor, M. Affatigato, S. A. Feller, Physical properties of alkaline-earth and alkali borate glasses prepared over an extended range of compositions, J. Non-Cryst. Solids 293 (2001) 669–675, https://doi.org/10.1016/S0022-3093(01)00768-2.

[64] I. Mills, T. Cvitas, K. Homann, N. Kallay, K. Kuchitsu, Quantities, Units and Symbols in Physical Chemistry, Second ed., Blackwell Science Ltd, Oxford, 1993.

[65] S. Giri, C. Gaebler, J. Helmus, M. Affatigato, S. Feller, M. Kodama, A general study of packing in oxide glass systems containing alkali, J. Non-Cryst. Solids 347 (1–3) (2004) 87–92, https://doi.org/10.1016/j.jnoncrysol.2004.08.103.
[66] J.E. Shelby, Thermal-expansion of alkali borate glasses, J. Am. Ceram. Soc. 66 (3) (1983) 225–227, https://doi.org/10.1111/j.1151-2916.1983.tb10023.x.
[67] Y.D. Yiannopoulos, G.D. Chryssikos, E.I. Kamitsos, Structure and properties of alkaline earth borate glasses, Phys. Chem. Glasses 42 (3) (2001) 164–172.
[68] V. Dimitrov, T. Komatsu, An interpretation of optical properties of oxides and oxide glasses in terms of the electronic ion polarizability and average single bond strength (review), J. Univ. Chem. Technol. Metall. 45 (3) (2010) 219–250.
[69] K.H. Sun, Fundamental condition of glass formation, J. Am. Ceram. Soc. 30 (9) (1947) 277–281, https://doi.org/10.1111/j.1151-2916.1947.tb19654.x.
[70] A. Makishima, J.D. Mackenzie, Direct calculation of Young's moidulus of glass, J. Non-Cryst. Solids 12 (1) (1973) 35–45, https://doi.org/10.1016/0022-3093(73)90053-7.